Comparison of Magma Activities in the Rembrandt and Caloris Interior Smooth Plains on Mercury: Implications for the Lateral Heterogeneity in Magma Activity. K. Hirata[1,2], T. Morota[1], S. Sugita[1], C. M. Ernst[3], and T. Usui[2], [1]The University of Tokyo, 7-3-1 Hongo, Bunkyo, Tokyo, Japan (hirata-kaori444@g.ecc.u-tokyo.ac.jp), [2]Institute of Space and Astronautical Science, JAXA, 3-3-1 Yoshinodai, Sagamihara, Kanagawa, Japan, [3]The Johns Hopkins University Applied Physics Laboratory, Laurel, MD 20723, USA.

Introduction: Observations of the surface of Mercury by Mariner 10 and MESSENGER have revealed that ~27% of the surface is occupied by smooth plains [e.g.,1] and that smooth plains area in the northern hemisphere was approximately seven times larger than the southern hemisphere [2,3]. On the Moon, there is a near-farside asymmetry in volcanic materials [4], being attributed to differences in two independent factors, the thickness of low-density anorthosite crust [e.g.,5] and the magma production due to heat-producing element distribution [e.g.,6]. In contrast, the cause of the north-south asymmetry in smooth plains on Mercury is poorly understood due to the lack of available data. Crustal thickness models [7] show that smooth plains are preferentially located in the parts of thin crust, suggesting that magma is more likely to erupt to the thinner crust [3]. To evaluate how crusts and lateral heterogeneity in magma production contribute to north-south asymmetry, it is necessary to estimate the volumes of erupted magmas and investigate the relation between the degree of magma activity and crustal thickness.

To date, many studies have measured crater size-frequency distributions (CSFDs) and shown that most smooth plains are formed 3.5-3.8 Ga [e.g.,2,3,8,9]. However, these studies adopted different approaches (e.g., chronology model), resulting in a difficulty to reliably compare the results. This study reevaluated the CSFDs and the volumes of volcanic materials for the Rembrandt and Caloris plains, in the southern and northern hemispheres, respectively, on a single measurement condition, and determined the magma eruption rates.

Method: The surface ages were estimated from CSFDs on the target surface using the chronology model [10]. Generally, a CSFD runs along a single isochron indicating the surface formation age, however, in some cases, a CSFD may exhibit a kink and run along multiple isochrones within different crater-diameter ranges, suggesting partial resurfacing by multiple magma eruptions. The crater diameter related to the kink was used to estimate the thickness of surface units based on the diameter-rim height scaling relation [11]. The CSFDs of crater diameters lower and higher than the kink yield the ages of the surface and underlying lava, respectively.

The color properties of the ejecta and interior of each crater were examined, following Ernst et al. [12], to determine whether the crater excavated the LRM layer beneath the HRP layers or not, using the enhanced color map [13]: Blue and yellow materials relate to the LRM and HRP material, interpreted as the original basin floor and the volcanic infill, respectively [14].

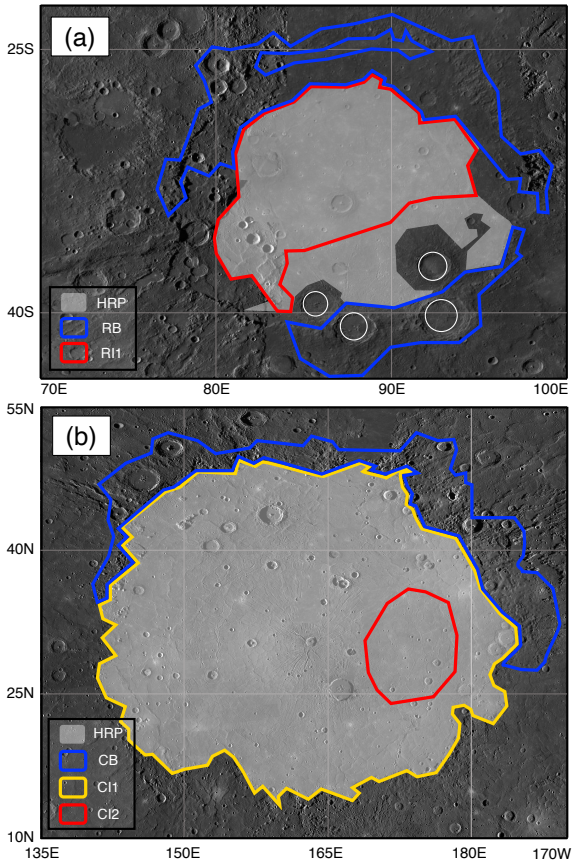

Figure 1. Study area within (a) the Rembrandt basin and (b) the Caloris basin shown on the monochrome base map. The areas exterior to the basin rims (blue; RB and CB) were considered basin rim materials. Those interior to the basin rim (red and yellow; RI1, CI1, and CI2) were considered interior smooth plains. Note that RI1 excluded the southeastern half of the basin interior area to prevent contamination of secondary craters from large craters outlined in white circles in (a).

Rembrandt Basin: The Rembrandt basin (33°S, 87°E) is the largest impact basin (~710 km in diameter) in the southern hemisphere [3]. The basin formation and magma eruption ages were estimated from the CSFDs in the exterior area (Rembrandt Basin material: RB) [8] and the interior area (Rembrandt Interior plain: RI1), with the southern regions being excluded to avoid contamination of secondary craters (Fig. 1(a)). The CSFD in RB suggested the basin formation ages of 3.93

Gy, and that in RI1 exhibited a kink, implying the resurfacing by multiple eruptions. The Rembrandt eruption ages were estimated from 3.87 to 3.76 Gy (Table 1). Two distinct volcanic deposit layers (R-HRP1 and 2) were detected, whose thickness was estimated to be 0.9-2.2 km in total from the crater color investigation, consistent with the previous estimate [9].

Caloris Basin: The Caloris basin (32°N, 163°E) has a diameter of ~1550 km [15]. To estimate the basin formation and magma eruption ages, the CSFDs were measured on the northern rim materials (Caloris Basin material: CB) [16] and the interior areas (Caloris Interior plain: CI1 and CI2) (Fig. 1(b)). To prevent contamination of secondary craters, CI2 was selected for measurement of craters >2.5 km in diameter. The estimated formation age and magma eruption ages were 3.94 Gy and 3.88-3.74 Gy, respectively (Table 1). In the Caloris basin, three distinct volcanic layers were detected. This study adopted the HRP material thickness of 2.5-3.5 km estimated by Ernst et al. [12].

Magma Eruption Rates: The magma eruption rates (MERs) were determined from the eruption ages, the thicknesses of the HRP layers, and the total thickness of the HRP materials. Considering the uncertainties, we estimated the conservative minimum and maximum of the MERs (Table 2). The time averages of MERs were yielded by dividing the full volume of volcanic infill by the period spanning from basin formation to the youngest eruption estimated in this study. The time-averaged MERs within the Caloris basin were at most approximately three times that for the Rembrandt basin.

Effect of Crustal Thickness on Magma Eruption: The crustal thickness model suggested ~20 km- and ~50 km-thick crusts within and around the Caloris basin, respectively [7]. As the crustal thickness in the Rembrandt area could not be resolved due to the spatial resolution, we estimated it assuming a spatially uniform 50 km-thick crust before impact events, where the Caloris-forming impact removed the upper 30 km of the crust. As the size of the Rembrandt is approximately half the Caloris, it was inferred that the Rembrandt impact event formed a 35 km-thick crust by excavating the upper 15 km of the crust. The observed difference of MER within the two areas may be attributed to differences in crustal thickness.

By assuming that the magma eruptions within the Rembrandt and Caloris basins represent the southern and northern hemispheres, respectively, we evaluated the influence of crustal thickness on the north-south dichotomy in a smooth plain distribution from the observed difference in MERs within the two basins. The lateral difference in time-averaged MERs within large basins (<3 times) is smaller than that in the smooth plain distribution (~7 times), suggesting the necessity of the effect of the crustal thickness for explaining the asymmetric distribution of smooth plains, even if the observed difference in MERs is due to the difference in the magma production in the mantle, which is consistent with the crustal thickness model [7] showing the asymmetric crustal thickness between two hemispheres. This idea suggests that the difference in magma production in the mantles between the northern and southern hemispheres is not significant unlike the Moon [e.g.,6], which implies the absence of large regional variation in the heat-producing elements in Mercury's mantle.

Table 1. Observed crater densities $N(10)$ and model ages within the measurement areas.

Units	Materials	Area [$\times 10^6$ km^2]	$N(10)$ [10^{-6} /km^2]	Age [Gyr]	Fitting Diameter [km]
Rembrandt basin					
RB	Basin Rim	0.192	78 ± 21	$3.93^{+0.03}_{-0.06}$	$50 - 100$
RI1	Interior Plain	0.169	106 ± 26	$3.80^{+0.02}_{-0.03}$	$15 - 30$
				$3.76^{+0.01}_{-0.01}$	$3 - 10$
Caloris basin					
CB	Basin Rim	0.340	58 ± 14	$3.94^{+0.03}_{-0.04}$	$50 - 100$
CI1	Interior Plain	1.726	80 ± 7	$3.80^{+0.01}_{-0.02}$	$30 - 50$
				$3.76^{+0.01}_{-0.01}$	$13 - 20$
CI2	Interior Plain	0.131	68 ± 23	$3.74^{+0.01}_{-0.01}$	$3 - 10$

Table 2. Magma eruption periods and magma eruption rates (MERs) in each HRP layer within the Rembrandt and Caloris basins.

		Area [$\times 10^6$ km^2]	Period [Gyr]	MER [km/Gyr] min	MER [km/Gyr] max
Rembrandt	R-HRP1	0.229	0.13	2.6	12.5
	R-HRP2	0.229	0.04	11.6	13.7
	Total	0.229	0.17	5.2	12.3
Caloris	C-HRP1	1.73	0.14	7.6	16.1
	C-HRP2	1.73	0.04	4.8	6.5
	C-HRP3	1.73	0.02	26.5	28.0
	Total	1.73	0.20	9.3	15.1

References: [1] Murray, S. L. et al. (1974) *Science, 185(4146),* 169-179. [2] Byrne P. K. et al. (2016) *J. Geophys, Res, Planets, 118(6),* 1303-1322. [3] Denevi, B. W. et al. (2013) *J. Geophys, Res, Planets, 118(5),* 891-907. [4] Head J. W. (1976) *Rev. Geophys., 14(2),* 265-300. [5] Wilson, L. & Head, J. W. (2017) *Icarus, 283,* 146-175. [6] Laneuville, M. et al. (2013) *J. Geophys. Res. Planets, 118(7),* 1435-1452. [7] Smith. D. E. et al. (2012) *Science, 336(6078),* 214-217. [8] Ferrari, S. et al. (2015) *Geol. Soc. London, Spec. Publ., 401(1),* 159–172. [9] Semenzato, A. et al. (2020) *Remote Sens., 12(19),* 3213. [10] Le Feuvre, M. & Wieczorek, M. A. (2011) *Icarus 214(1),* 1435-1452. [11] Pike, R. J. (1988), *Mercury,* 165-273. [12] Ernst C. M. et al. (2015) *Icarus, 250,* 413-429. [13] Denevi, B. W. (2018) *Space Sci. Rev., 214(1)*, 1-52. [14] Whitten, J. L. & Head, J. W. (2015) *Icarus, 258,* 350-365. [15] Head, J. W. et al. (2009) *Earth Planet. Sci. Lett., 285(3-4),* 227-242. [16] Ernst, C. M. et al. (2017) *LPSC XLVIII,* 2934.